

Enhanced 3D Generation by 2D Editing

Haoran Li¹, Yuli Tian¹, Yong Liao^{1*}, Lin Wang², Yuyang Wang³, Peng Yuan Zhou⁴

¹University of Science and Technology of China, ²Nanyang Technological University

³The Hong Kong University of Science and Technology (Guangzhou), ⁴Aarhus University

{lhr123, yltian}@mail.ustc.edu.cn, yliao@ustc.edu.cn

eee-addison.wang@ntu.edu.sg, yuyangwang@hkust-gz.edu.cn, pengyuan.zhou@ece.au.dk

Abstract

Distilling 3D representations from pretrained 2D diffusion models is essential for 3D creative applications across gaming, film, and interior design. Current SDS-based methods are hindered by inefficient information distillation from diffusion models, which prevents the creation of photorealistic 3D contents. Our research reevaluates the SDS approach by analyzing its fundamental nature as a basic image editing process that commonly results in over-saturation, over-smoothing and lack of rich content due to the poor-quality single-step denoising. To address these limitations, we propose GE3D (3D Generation by Editing). Each iteration of GE3D utilizes a 2D editing framework that combines a noising trajectory to preserve the information of the input image, alongside a text-guided denoising trajectory. We optimize the process by aligning the latents across both trajectories. This approach fully exploits pretrained diffusion models to distill multi-granularity information through multiple denoising steps, resulting in photorealistic 3D outputs. Both theoretical and experimental results confirm the effectiveness of our approach, which not only advances 3D generation technology but also establishes a novel connection between 3D generation and 2D editing. This could potentially inspire further research in the field. **Code and demos are released at <https://jahnsonblack.github.io/GE3D/>.**

1. Introduction

Distilling 3D representations [17, 19–21, 27, 34, 37] from pretrained 2D text-to-image models [29] has garnered significant attention in the field of AI-generated content (AIGC). This method enables the generation of 3D representations from scratch based on user-provided text prompts, substantially reducing the workload for 3D modelers. Demonstrating vast potential, this technology promises wide-ranging applications across various industries, including gaming,

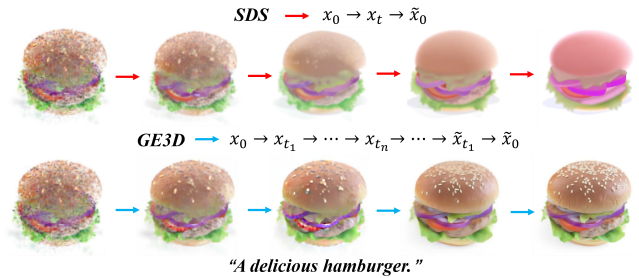


Figure 1. We simulate the 3D generation processes of SDS [27] and GE3D by inputting 2D coarse images through multiple iterations of single-step and multi-step editing. Here, x_0 is the input image, \tilde{x}_0 is the predicted image, and x_t and \tilde{x}_t are the latents along the noising and denoising trajectories, respectively. SDS, which relies on single-step editing, often leads to significant directional errors, resulting in images that are over-saturation and over-smoothing. In contrast, GE3D employs multi-step editing within each iteration, ensuring stable optimization and high-quality outcomes.

film production, and augmented/virtual reality (AR/VR).

Current research methodologies primarily adhere to Score Distillation Sampling (SDS) [27], a pioneering approach in the field of text-to-3D generation. This technique distills knowledge by matching the distribution of images rendered from 3D representations under random poses with that of a pretrained 2D large text-to-image diffusion model [29, 33], such as Stable Diffusion [29], under specific textual contexts. In the SDS process, noise is initially introduced to a rendered image in a single step. This noised image is then input into a diffusion model for denoising. The noise predicted by the diffusion model contains information derived from the input text. By reducing the discrepancy between the input and predicted noises, the 3D representation is optimized from the rendered viewpoint. Subsequent advancements in SDS-based methods [17, 19–21, 34, 37] for 3D generation have introduced a range of enhancements. These improvements include more advanced 3D representations [20, 34], optimized diffusion timesteps for sampling [12, 17], and refined

*Corresponding author

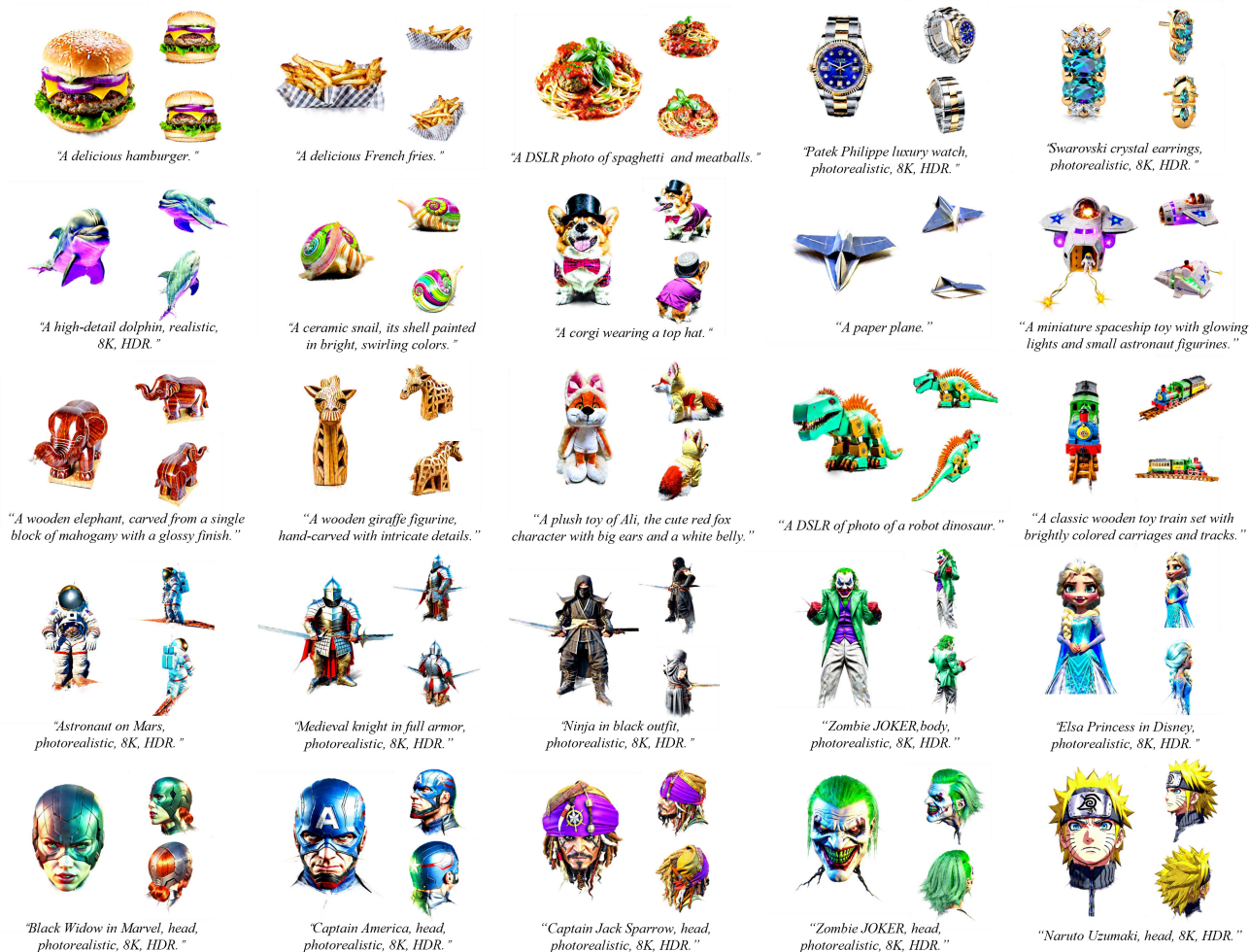


Figure 2. The text-to-3D generation results of our framework *GE3D*. *GE3D* replaced the inefficient single-step editing in SDS with multi-step 2D diffusion editing approach. This change resolves the issues of over-saturation and over-smoothing typically found in SDS-based generation methods, achieving photorealistic quality in 3D content generation. Please zoom in to see the details.

techniques for adding noise [19] in the SDS process. Despite these developments, challenges in generation quality, such as *over-saturation*, *over-smoothing*, and a *lack of content richness*, continue to persist.

We observed that the process used in SDS, which integrates information from pretrained 2D diffusion models through noising and denoising, bears similarity to 2D image editing [7, 15, 25], where the guided input image is methodically altered towards a specified textual direction. The key difference is that SDS employs a *single-step* editing process. However, traditional diffusion models typically require *multi-step* denoising, which involves adding information of varying granularities, to correct directional errors and generate high-quality images. This is because predicting the direction to x_0 in a single step often results in a substantial deviation from the true data trajectory. As illustrated in Figure 1, we simulate the SDS single-step image editing

process through multiple iterations on a coarse 2D image during the generation process. We observe that the content of the images progressively aligns with the textual prompt "A delicious hamburger," the quality of the generated images deteriorates: colors become overly saturated and textures become simpler and smoother. This degradation is attributed to significant errors in the predicted generation direction and the introduction of different random noises in each iteration, leading to varying predicted directions. These variations make the generation process unstable and tend to drive the outputs towards a simplistic mean direction associated with the text. As depicted in the lower section of Figure 1, high-quality image generation can be achieved by fully exploiting the multi-step denoising capabilities of diffusion models in each optimization iteration, thereby facilitating a comprehensive image editing process.

Therefore, we propose *GE3D*, a novel 3D generation

framework designed to produce photorealistic 3D content. This framework aligns the latents of the input images during the 2D diffusion editing process. In each iteration, we establish a noising trajectory to project the input image into high-dimensional diffusion space, accompanied by a denoising editing trajectory that incrementally incorporates information of varying granularities from the diffusion model. Larger timesteps impart coarse-grained information, while smaller timesteps contribute fine-grained details. By minimizing the differences in latents at corresponding timesteps along these trajectories, GE3D effectively distills multi-granularity information into the 3D representation. Additionally, we have developed a Gaussian coefficient function related to the number of iterations and denoising steps, optimizing the provision of coarse-grained information in initial phases and fine-grained information in later stages, thereby enhancing stability and efficiency in generation. The efficacy of GE3D in achieving photorealistic 3D generation is demonstrated in Figure 2.

Our main contributions can be summarized as follows:

- We conducted a comprehensive analysis of the relationship between 2D editing and 3D generation, demonstrating both qualitatively and quantitatively that the core of the SDS method lies in performing single-step editing during each optimization.
- We introduced a novel 3D generation framework, GE3D. By aligning the latents along the noising and denoising trajectories in each optimization step and integrating Gaussian weight coefficients, we achieved efficient and high-quality 3D generation.
- Both qualitative and quantitative results showcase the significant superiority of GE3D in generating photorealistic 3D representations that closely match text descriptions. This framework holds tremendous potential for applications across various 3D-related industries. Moreover, our work is expected to inspire further research that integrates advanced 2D editing techniques into the realm of 3D generation.

2. Related Works

2.1. Text-to-3D Generation

Current text-to-3D generation methods can be broadly categorized into two primary approaches: direct generation [11, 13, 26, 32, 40] and optimization-based generation [3, 17, 19–21, 27, 34]. Direct generation methods, such as Point-E [26], utilize a diffusion model to generate an image corresponding to the input text, subsequently training a transformation model to convert this image into a point cloud with a predetermined number of points. Alternatively, models like LRM [11], employ encoders to map text or images into 3D high-dimensional spaces, which are then decoded into specific 3D representations, such as meshes or 3D

Gaussians [16]. While these methods are capable of rapidly generating 3D representations, they involve high training costs and typically yield simpler 3D structures, which may not be suitable for complex 3D applications.

Optimization-based methods are capable of producing higher quality and more diverse 3D representations but generally require longer optimization times. Score Distillation Sampling (SDS) [27], a seminal work in this field, optimizes the process to ensure that images rendered from any camera pose conform to the distribution of a large pretrained text-to-image model. Building on SDS, subsequent research such as CSD [42] decomposes the SDS loss into classification and generative components, noting improvements in quality with generative loss alone. ProlifDreamer [37] introduced Variational Score Distillation (VSD), which treats 3D parameters as random variables and refines the distillation through particle sampling for model diversification. Consistant3D [39] utilizes fixed Gaussian noise to maintain consistency in the ordinary differential equation (ODE) sampling process. LucidDreamer [19] employs the DDIM [33] inversion method to enhance the consistency and quality of the optimization process. Further, DreamTime [12] demonstrate that different diffusion timesteps in a pretrained model offer variable information, with specific time sampling strategies significantly improving both quality and speed of generation. However, despite these advancements, these methods still struggle to produce photorealistic 3D content.

2.2. Text-based Image Editing

Current text-guided image editing methods generally involve two main stages. The first stage is image inversion, which involves mapping the image back to the latent space of a generative model (such as GANs [5, 14] or diffusion models [10, 29, 33]) through a reconstruction loss. The second is editing that the latents is guided by a new text in latent space and then achieves final modifications in image space while preserving most of the original content. For GAN-based methods [1, 35, 36], an encoder [35, 38] is typically trained to map images to latents, and the latents are precisely obtained through optimization techniques [18]. For methods based on diffusion models, such as Imagic [15], precise reconstruction is achieved by optimizing the alignment of the target text embedding with the image embedding, though this usually requires retraining the diffusion model at a high cost. In advanced techniques, tuning-free methods like DDIM [33] Inversion can approximate the inversion trajectory through deterministic sampling, but this method often results in reconstruction images that deviate from the input image, thereby affecting subsequent editing. Null-text Inversion(NTI) [25] optimizes a differentiable empty text embedding to align the noising and denoising processes for more precise reconstruction. Meanwhile, Negative Prompt Inversion(NPI) [24] eliminates the optimization process used

in NTI and directly uses the prompt of input image as an approximate substitute, which is faster but gets some reconstruction errors. Prompt Tuning Inversion (PTI) [4] achieves precise reconstruction without explicitly inputting the image prompt by optimizing the prompt during the denoising process. Once the deterministic diffusion trajectories are obtained, image editing based on new text can be completed through interpolation of text embeddings during the generation process or using the Prompt2Prompt [7] technique.

We integrate the image inversion and editing stages to enhance the efficiency of 3D generation process.

3. Methods

3.1. Preliminary

Diffusion models [10, 29, 33] generate data by estimating the denoising gradient direction of the current state distribution. During training, the model first adds t -timestep gaussian noise ϵ to the input data x and get x_t :

$$x_t = \sqrt{\bar{\alpha}_t}x + \sqrt{1 - \bar{\alpha}_t}\epsilon. \quad (1)$$

Then it learns a noise prediction network ϕ by minimizing the loss between the predicted $\epsilon_\phi(x_t, t)$ noise and the actual noise ϵ :

$$\mathcal{L}_t = \mathbb{E}_{x, \epsilon \sim \mathcal{N}(0, I)} \left[\|\epsilon_\phi(x_t, t) - \epsilon\|^2 \right]. \quad (2)$$

In the inference process, it predicts and removes noise step by step to complete the data generation.

DDIM sampling [33] is used to estimate the relationship between any two noised latents, so it is often commonly employed to accelerate the inference process. We can transform x_m to x_k (no matter $m > k$ or $m < k$) using DDIM sampling (we set the coefficient of random perturbation $\delta_t = 0$ in [33]) by:

$$x_k = \sqrt{\bar{\alpha}_k} \frac{x_m - \sqrt{1 - \bar{\alpha}_m} \epsilon_\phi(x_m, m)}{\sqrt{\bar{\alpha}_m}} + \sqrt{1 - \bar{\alpha}_k} \epsilon_\phi(x_m, m). \quad (3)$$

Classifier-Free Guidance (CFG) [9] is a technique used during generation to enable text-guided synthesis without relying on an explicit classifier. It introduces a mechanism where both unconditional and conditional generation collaboratively control the image generation. The formulation is as follows:

$$\tilde{\epsilon}_\phi(x_t, t, y, \emptyset) = \epsilon_\phi(x_t, t, \phi) + \omega(\epsilon_\phi(x_t, t, y) - \epsilon_\phi(x_t, t, \emptyset)), \quad (4)$$

where y represents the conditional text embedding derived from the input prompt and \emptyset represents the unconditional empty text embedding. ω represents the guidance coefficient. A higher value of ω increases conformity to the text y but may decrease the quality of the generated images.

Score Distillation Sampling (SDS) [27] aims to distill information from a pretrained 2D text-to-image diffusion model.

Initially, a camera pose c is randomly selected to render a differentiable 3D representation [16, 22, 31] θ using rendering function $g(\theta, c)$ to obtain an image x . Random t -timestep noise is then added to x , and denoised by ϕ . The 3D representation is updated by minimizing the difference between these two noises:

$$\nabla_\theta \mathcal{L}_{\text{SDS}}(\theta) = \mathbb{E}_{t, \epsilon, c} \left[f(t) (\tilde{\epsilon}_\phi(x_t, t, y, \emptyset) - \epsilon) \frac{\partial g(\theta, c)}{\partial \theta} \right], \quad (5)$$

where $f(t)$ serves as a weighting function that adjusts based on the timesteps t . In SDS, the CFG coefficient is set to 100.

3.2. Text-based 2D editing vs. SDS text-to-3D tasks

Qualitative analysis. Text-based 2D editing tasks [1, 4, 7, 15, 24, 25, 35, 36] are essentially image-to-image tasks. The original image is input into a pretrained text-to-image model, mapping it to a high-dimensional latent space through a noising trajectory, and then gradually adding information from the editing text through a denoising trajectory to achieve editing. The edited image need retaining most of the content from the original image. Similarly, text-to-3D methods [3, 17, 19–21, 27, 34] based on SDS [27] also leverage the prior knowledge of a pretrained text-to-image model, incorporating this information into a differentiable 3D representation [16, 22, 31]. During each step of optimization, an image is rendered under a random camera pose and then input into a pretrained diffusion model which is similar to the input process in editing tasks. By minimizing the noise difference between single-step noising and denoising, text information is gradually incorporated. This process mirrors editing tasks, where editing information is incrementally introduced through denoising. Thus, text-to-3D can be viewed as invoking a text-guided editing task at each optimization step.

Quantitative analysis. In a Text-based 2D editing task, the input image x is typically inverted first through an alignment process. We define a diffusion trajectory for noising as $\{x_{t_0}, x_{t_1}, \dots, x_{t_{n-1}}, x_{t_n}\}$ ($x = x_{t_0}, t_n > t_{n-1} > \dots > t_1 > t_0$) and a denoising trajectory $\{\tilde{x}_{t_{n-1}}, \dots, \tilde{x}_{t_1}, \tilde{x}_{t_0}\}$. We need to progressively align the corresponding latents x_{t_i} and \tilde{x}_{t_i} ($i = 0, \dots, n - 1$) to achieve inversion. Methods such as NTI [25] and PTI [4] use differentiable embeddings for the unconditional empty text \emptyset_t or the conditional text y_t during the denoising process, enabling optimization for alignment. We represent this process as:

$$\alpha_{t_i} = \arg \min_{\alpha_{t_i}} \|x_{t_{i-1}} - \tilde{x}_{t_{i-1}}(\tilde{x}_{t_i}, t_i, \alpha_{t_i})\|_2^2, \quad (6)$$

where $i = n, \dots, 1$ and $\alpha_{t_i} = \emptyset_{t_i}$ or y_{t_i} . And after this alignment process, the new text embedding y_{edit} can be combined with the optimized embedding sequence α_{t_i} ($i = 1, \dots, n$) to perform editing.

For SDS, similarly to many method analyses [12, 19], we directly add noise using Eq. 1 to x_{t_0} across t_n -timestep and

then use Eq. 3 for denoising in just one step to get \tilde{x}_{t_0} , we can derive the following formula:

$$\begin{cases} x_{t_n} = \sqrt{\bar{\alpha}_{t_n}}x_{t_0} + \sqrt{1 - \bar{\alpha}_{t_n}}\epsilon \\ \tilde{x}_{t_0} = \frac{x_{t_n} - \sqrt{1 - \bar{\alpha}_{t_n}}\tilde{\epsilon}_\phi(x_{t_n}, t_n, y, \emptyset)}{\sqrt{\bar{\alpha}_{t_n}}} \end{cases} \quad (7)$$

By eliminating x_{t_n} , we can obtain:

$$\sqrt{\frac{\bar{\alpha}_{t_n}}{1 - \bar{\alpha}_{t_n}}}(x_{t_0} - \tilde{x}_{t_0}) = \tilde{\epsilon}_\phi(x_{t_n}, t_n, y, \emptyset) - \epsilon, \quad (8)$$

where $\tilde{\epsilon}_\phi(x_{t_n}, t_n, y, \emptyset) - \epsilon$ is the core of SDS in Eq. 5.

LucidDreamer [19] is currently the state-of-the-art (SOTA) method. Its ISM replaces $\tilde{\epsilon}_\phi(x_t, t, y, \emptyset) - \epsilon$ in SDS with $\tilde{\epsilon}_\phi(x_t, t, y, \emptyset) - \epsilon_\phi(x_s, s, \emptyset)$ where x_t is obtained by adding noise to x_s using DDIM Inversion. We set $t_{n-1} = s$, $t_n = t$ and add noise through $x_{t_{n-1}}$ to get x_{t_n} , and then denoise from x_{t_n} to retrieve $\tilde{x}_{t_{n-1}}$ by Eq. 3. The equations in this process can be expressed as follows:

$$\begin{cases} \frac{x_{t_n}}{\sqrt{\bar{\alpha}_{t_n}}} = \frac{x_{t_{n-1}}}{\sqrt{\bar{\alpha}_{t_{n-1}}}} + \delta_{t_n}\epsilon_\phi(x_{t_{n-1}}, t_{n-1}, \emptyset) \\ \frac{\tilde{x}_{t_{n-1}}}{\sqrt{\bar{\alpha}_{t_{n-1}}}} = \frac{x_{t_n}}{\sqrt{\bar{\alpha}_{t_n}}} - \delta_{t_n}\tilde{\epsilon}_\phi(\tilde{x}_{t_{n-1}}, t_n, y, \emptyset), \end{cases} \quad (9)$$

where $\delta_{t_n} = \sqrt{\frac{1 - \bar{\alpha}_{t_n}}{\bar{\alpha}_{t_n}}} - \sqrt{\frac{1 - \bar{\alpha}_{t_{n-1}}}{\bar{\alpha}_{t_{n-1}}}}$. By adding the two equations and eliminating x_{t_n} , we can obtain:

$$\frac{x_{t_{n-1}} - \tilde{x}_{t_{n-1}}}{\sqrt{\bar{\alpha}_{t_{n-1}} \cdot \delta_{t_n}}} = \tilde{\epsilon}_\phi(\tilde{x}_{t_{n-1}}, t_n, y, \emptyset) - \epsilon_\phi(x_{t_{n-1}}, t_{n-1}, \emptyset). \quad (10)$$

Thus, based on Eq. 6, Eq. 8 and Eq. 10, we can observe that SDS and ISM essentially align the latents x_{t_i} ($i = 0$ or $n - 1$) at different timesteps along the diffusion trajectory of inversion process in 2D editing task. We will provide more information in the Supplementary Materials regarding the connections between current 3D generation methods and 2D editing methods.

3.3. GE3D

As discussed in the previous section, we can see that current methods based on SDS essentially only provide denoising information for a single step as shown in right part of Figure 3. In contrast, traditional diffusion models rely on multi-step denoising, which integrates information at different granularities for high-quality generation. During the early denoising stages, the model captures coarse-grained details (e.g., position and general shape of objects), while later stages refine fine-grained details (e.g., object edges). Consequently, in 2D editing tasks, aligning information across multiple denoising steps is crucial for achieving accurate image inversion and ensuring high-quality image editing.

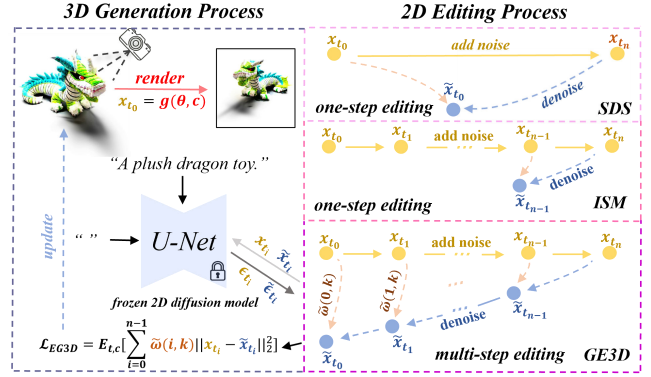


Figure 3. The overview of GE3D. We integrated the 2D editing process into 3D generation. Unlike the single-step editing in SDS in DreamFusion [27] and ISM in LucidDreamer [19], we used multi-step editing with latents alignment to combine different granularities of information from the pre-trained 2D diffusion model into the 3D representation, achieving high-quality generation.

Thus, we fully integrate the 2D editing task with the 3D generation task as shown in Figure 3. In each iteration of 3D generation, we apply a multi-step denoising editing process to extract rich semantic features (both coarse-grained and fine-grained), and then align the latents at the noised and corresponding denoised nodes using the reconstruction method like Eq. 6 to achieve high-quality 3D representation generation. Specifically, similar to 2D editing tasks, we define an n -step noising trajectory and a corresponding reverse denoising trajectory. During the noising process, we employ an ODE-guided DDIM process with empty text embeddings to preserve the features of the input image. In the denoising process, we use the guidance information calculated by Eq. 4 and obtain a sequence of semantic information with varying granularities through the stepwise denoising process. We then use L_2 loss to align the corresponding latents along the two trajectories:

$$L_i = \|x_{t_i} - \tilde{x}_{t_i}\|_2^2, i = 0, \dots, n - 1. \quad (11)$$

This forces the 3D representation to learn rich semantic information at different granularities from the current viewpoint, resulting in the generation of high-quality 3D content.

We also introduce $\omega(i, k)$ to represent the coefficient applied to the loss L_i in the k -th iteration. We aim for a higher $\omega(i, k)$ contribution from coarse-grained losses L_i (large i) when k is small, as the shape of 3D representation has not yet been optimized, and overly fine-grained information (small i) could interfere its rich semantic information. During the early stages of optimization, coarse-grained information is primarily used. As the optimization progresses, the contribution of L_i (large i) becomes less beneficial for 3D generation, and more fine-grained information (small i) is needed to achieve high-quality results.

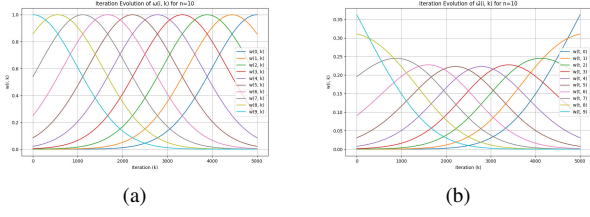


Figure 4. (a) shows the $\omega(i, k)$ function plots for different granularities (i) and iteration counts (k), while (b) shows the normalized version of the plots.

We use multiple Gaussian functions to model the characteristic where the coefficient first increases and then decreases. For each $\omega(i, k) = \exp(-\frac{(k-\Delta_i)^2}{2\sigma^2})$ where Δ_i represents the iteration number at which the peak occurs of i -th Gaussian function. So, for the endpoints $\Delta_{n-1} = 0$ and $\Delta_0 = K$ (K denotes the total number of iterations). We set Δ_i at equal intervals as follows:

$$\Delta_i = (n - i - 1) \times \frac{K}{n - 1}, i = 0, \dots, n - 1. \quad (12)$$

We need to set a large value (1000) for σ to ensure that information at different granularities participates in the optimization process within each iteration, as shown Figure 4a (we set $n = 10, k = 5000$). We normalize all the coefficients $\omega_{i,k}$ at the same iteration k as follows:

$$\tilde{\omega}(i, k) = \frac{\omega(i, k)}{\sum_{i=0}^{n-1} \omega(i, k)}. \quad (13)$$

And Figure 4b shows the function plot after normalization of the $\tilde{\omega}(i, k)$. Thus, the loss for GE3D can be expressed as:

$$L_{GE3D} = \mathbb{E}_{t,c} \left[\sum_{i=0}^{n-1} \tilde{\omega}(i, k) \|x_{t_i} - \tilde{x}_{t_i}\|_2^2 \right]. \quad (14)$$

Our complete algorithmic process is shown in Algorithm. 1.

Our method uncovers the essence of SDS by using a single-step denoising process for coarse editing. In this sense, SDS can be viewed as a subset of our approach, meaning that many improvements and techniques developed for SDS can be seamlessly applied to our method. For instance, we can directly integrate the denoising formula from Perp-Neg [2] to mitigate the Janus (multi-head) problem. Similarly, we can replace the single-step denoising in Reconstructive Generation from Formation Pattern Sampling [17] with multi-step editing to accelerate surface texture generation. Additional details are available in the supplementary materials.

4. Experiment

Implementation Details. For the 3D representations, we opted for 3D Gaussians [16] due to their explicit nature,

Algorithm 1 GE3D

- 1: **Input:** diffusion timestep trajectory $\{t_0, t_1, \dots, t_n\}$, iteration number K , target text embedding y , and null text embedding \emptyset .
 - 2: **for** $k = [0, \dots, K - 1]$ **do**
 - 3: $x_{t_0} = g(\theta, c)$
 - 4: **for** $i = [0, \dots, n - 1]$ **do**
 - 5: $\Delta_i = (n - i - 1) \times \frac{K}{n - 1}$
 - 6: $\omega(i, k) = \exp(-\frac{(k-\Delta_i)^2}{2\sigma^2})$
 - 7: $\tilde{\omega}(i, k) = \frac{\omega(i, k)}{\sum_{i=0}^{n-1} \omega(i, k)}$
 - 8: $\epsilon_\phi(x_{t_i}, t_i, \emptyset) = \text{U-Net}(x_{t_i}, t_i, \emptyset)$
 - 9: $\delta_{t_{i+1}} = \sqrt{\frac{1-\bar{\alpha}_{t_{i+1}}}{\bar{\alpha}_{t_{i+1}}}} - \sqrt{\frac{1-\bar{\alpha}_{t_i}}{\bar{\alpha}_{t_i}}}$
 - 10: $x_{t_{i+1}} = \sqrt{\bar{\alpha}_{t_{i+1}}} (\frac{x_{t_i}}{\sqrt{\bar{\alpha}_{t_i}}} + \delta_{t_{i+1}} \epsilon_\phi(x_{t_i}, t_i, \emptyset))$
 - 11: **end for**
 - 12: $\tilde{x}_{t_n} = x_{t_n}$
 - 13: **for** $i = [n - 1, \dots, 0]$ **do**
 - 14: $\tilde{\epsilon}_\phi(\tilde{x}_{t_{i+1}}, t_{i+1}, y, \emptyset) = \text{U-Net}(\tilde{x}_{t_{i+1}}, t_{i+1}, y, \emptyset)$
 - 15: $\tilde{x}_{t_i} = \sqrt{\bar{\alpha}_{t_i}} (\frac{\tilde{x}_{t_{i+1}}}{\sqrt{\bar{\alpha}_{t_{i+1}}}} - \delta_{t_{i+1}} \tilde{\epsilon}_\phi(\tilde{x}_{t_{i+1}}, t_{i+1}, y, \emptyset))$
 - 16: **end for**
 - 17: $\nabla_\theta L_{GE3D} = \sum_{i=0}^{n-1} \tilde{\omega}(i, k) (x_{t_i} - \tilde{x}_{t_i})$
 - 18: Update θ
 - 19: **end for**
-

which offers greater potential for applications, compared to other 3D representation techniques [22, 31]. We utilized Point-E [26] to generate initial sparse Gaussian point clouds of objects. For the 2D text-to-image diffusion models, we employed Stable Diffusion 2.1 [29]. In our diffusion trajectory, we defined time nodes ranging from 5 to 10, with step intervals between nodes set at 40 to 60, 60 to 80, and 80 to 100. We set the classifier-free guidance (CFG) coefficient to 7.5. To ensure a fair comparison, we conducted tests for GE3D and all baseline methods using the same NVIDIA A6000 GPU.

Baselines. For the comparative analysis of text-to-3D generation, we utilize the current open-sourced state-of-the-art(SOTA) methods as our baselines: DreamFusion [27], Magic3D [20], ProlificDreamer [37], GaussianDreamer [41] and LucidDreamer [19]. (DreamFusion, ProlificDreamer and Magic3D have been reimplemented by Three-studio [6]).

Evaluation Metrics. We use CLIP similarity [28] to measure the alignment between the rendered image of the generated 3D representation and their corresponding text descriptions. Additionally, for assessing the quality of generated 3D representations, we calculate the Fréchet Inception Distance (FID) [8] between the rendered images and real-world images, as well as using the Blind/Referenceless Image Spatial Quality Evaluator (BRISQUE) [23]. For all quantitative comparison experiments, we generated 100 3D

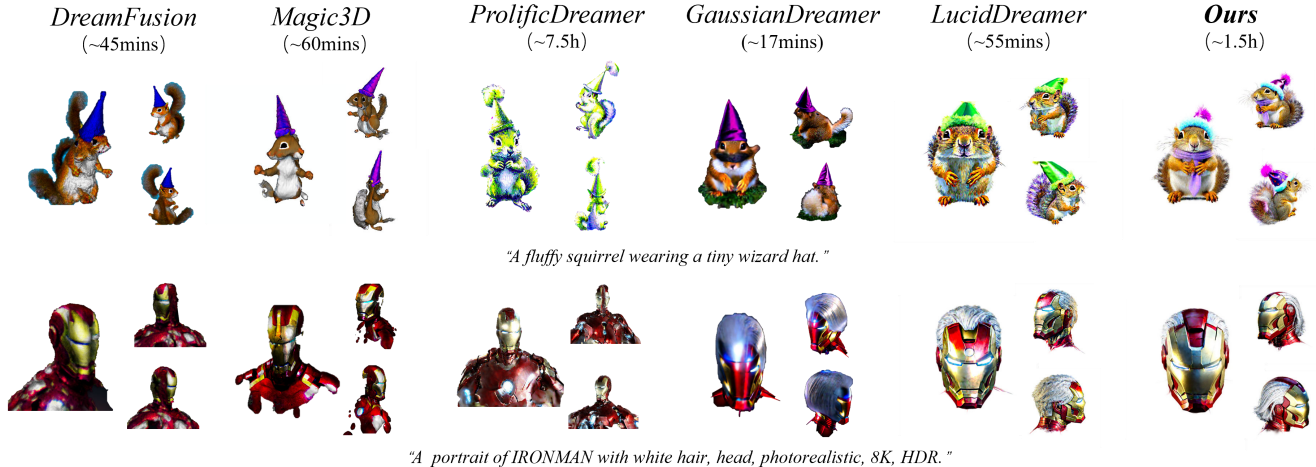


Figure 5. Qualitative comparison with baselines in text-to-3D generation.

representations for each text prompt across all baselines, randomly sampling 20 images from each set and computing the aforementioned metrics.

4.1. Qualitative Results

Figure 2 qualitatively showcases the results of GE3D across the generation of various types of 3D objects. By employing a multi-step 2D editing process in each iteration, our framework fully leverages the capabilities of large pretrained 2D diffusion models [29]. As shown, GE3D not only generates photorealistic results for categories such as animals, luxury goods, and dolls, but it also excels in more challenging tasks, such as generating 3D avatars and human faces, with results that are nearly indistinguishable from real-world images.

Figure 5 presents a qualitative comparison between our method and other baseline approaches. As demonstrated, our generated 3D representations significantly outperform other methods [19, 20, 27, 37, 41] in terms of quality. For the prompt "A fluffy squirrel wearing a tiny wizard hat", our method produces fur that appears more lifelike and hat details that are clearer, resulting in a more realistic overall appearance. For the prompt "A portrait of IRONMAN with white hair, head, photorealistic, 8K, HDR", our results and those from LucidDreamer [19] are closer to the text prompt than those from other methods. However, LucidDreamer’s output displays many surface artifacts. This issue stems from LucidDreamer’s ISM [19] method, which relies on single-step editing within a diffusion model, as discussed in Section 3.2. Consequently, ISM-generated 3D representations lack fine details. In contrast, our 3D outputs showcase enhanced details, eliminate artifacts, and improve lighting effects, achieving superior photorealistic quality.

It is worth noting that due to the comprehensive editing process employed in each iteration, our method takes

Table 1. Quantitative results of GE3D compared with baselines. \uparrow means the larger the better while \downarrow means the smaller the better.

	CLIP Similarity		FID \downarrow	BRISQUE \downarrow
	ViT-L/14 \uparrow	ViT-BigG/14 \uparrow		
Dreamfusion [27]	0.278	0.370	265.57	86.58
Magic3D [20]	0.262	0.351	285.20	79.74
ProlificDreamer [37]	0.287	0.399	254.53	74.16
GaussianDreamer [41]	0.286	0.396	244.48	86.91
LucidDreamer [19]	0.290	0.402	199.19	60.22
Ours	0.298	0.423	148.33	46.99

longer to achieve the highest quality compared to other baselines. However, even with extended optimization time, these baselines cannot achieve the same level of generated quality as ours. Additionally, because they rely on single-step editing, their 3D representations gradually degrade into over-saturation and over-smoothing results as optimization time increases. For more related qualitative demonstrations, particularly comparisons with LucidDreamer, please refer to our supplementary materials.

4.2. Quantitative Results

In Table 1, the CLIP similarity results indicate that our generated 3D representations more closely align with the input text prompts a benefit derived from the multi-step editing process in each optimization that incorporates richer textual information. Additionally, the quantitative assessments from FID and BRISQUE scores further confirm that our method produces 3D contents of superior generative quality.

4.3. Convergence Speed Analysis

Figure 6 illustrates the optimization results across different iterations k . Our method, GE3D, produces satisfactory results within 500 to 1000 iterations, requiring less time than the baselines [19, 20, 27, 37, 41], which generate lower-quality

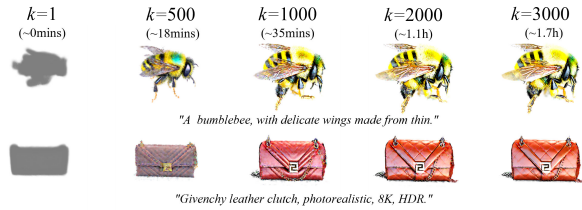


Figure 6. The result of convergence speed in GE3D.

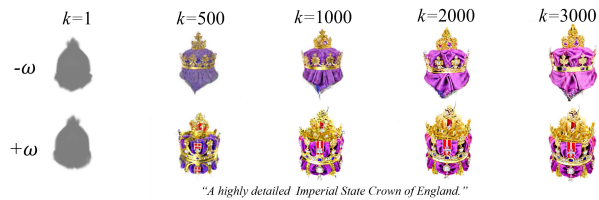


Figure 7. The result of using ω with GE3D.

outputs. This enhanced efficiency is due to the ω function in GE3D, which optimizes the information flow during the process, enabling quicker convergence from coarse to fine details.

Further, Figure 7 delves into how the ω coefficient affects the convergence speed and generation quality. With the ω function, GE3D significantly improves optimization speed, achieving desired results in a shorter time by effectively regulating the transition of details, thus facilitating a more sequential and refined generation process.

4.4. Ablation Study

As shown in Figure 8, we conducted an ablation study to analyze the impact of the farthest timestep and step sizes in the GE3D generation process. The vertical axis represents the farthest timestep, while the horizontal axis indicates the step sizes during each noising and denoising process. In this experiment, the ω coefficient was not used, and the time shown reflects the optimization completion time. Our findings highlight that *the ratio of the farthest timestep to the step size- referred to as the number of steps n-is critical for 3D generation*. When n is too small, optimization is prone to failure (as seen in the lower-right corner), because the diffusion model provides insufficient guidance for generating 3D representations. On the other hand, when n is too large, the results degrade in quality (as shown in the upper-left corner). Although more steps lead to finer details, excessive information from the diffusion model causes instability in the optimization process (from the 2D editing perspective, this is because the editing result diverges too much from the input image, leading to a lack of consistency of the input information). This instability stems from excessive divergence from the input image, disrupting consistency and exacerbating the Janus (multi-head) prob-

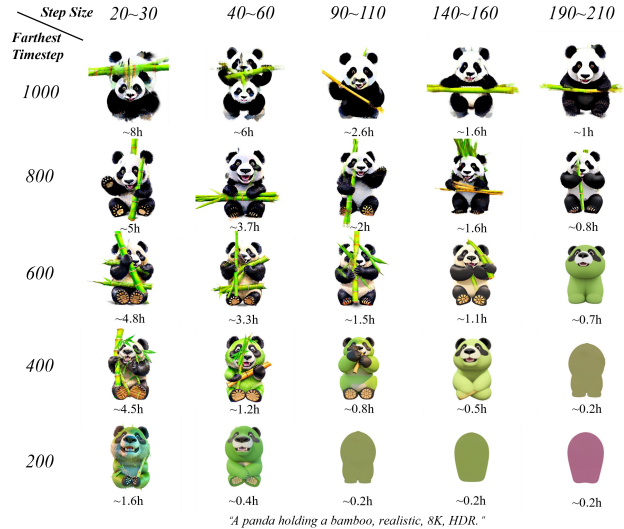


Figure 8. Ablation result of the farthest timestep and step sizes.



Figure 9. The limitation of GE3D for generating the small head of avatar. It cannot generate as finely as when only generating a human head.

lem in 3D generation. We found that around 5 to 10 steps typically yields the best results, as shown along the diagonal of the graph. This range provides a balanced flow of stable and rich guidance information. Interestingly, the lower-left corner of the graph shows that even with multiple steps using diffusion information from timesteps 0 to 200, we can still generate valid 3D representations. This challenges the common belief in prior work [12] that smaller step sizes cause instability and failure. Thus, *the key to successful text-to-3D generation lies in ensuring the pre-trained diffusion model provides sufficient information, which can be achieved through multi-step editing*. However, relying solely on fine-grained information may lead to semantically inconsistent outputs, such as the green panda. Therefore, selecting an optimal farthest timestep to balance both coarse and fine-grained information is crucial for generating high-quality and semantically coherent 3D representations.

We have included additional experiments and details of the generation process in the supplementary materials.

5. Limitation, Future Work and Conclusion

The multi-step editing process in GE3D inherently involves a time cost. While generating coarse representations is fast, most time is spent fine-tuning surface details as discussed

in Section. 4.3. We plan to improve this process for better efficiency. Additionally, when generating avatars, the head often appears too small to be optimized with the same level of detail as the body, leading to blurry outputs as shown in Figure 9. To address this, we are developing a specialized camera sampling algorithm that ensures finer facial detail while optimizing the entire digital human.

We analyze the relationship between 3D generation and 2D editing, integrating them into a novel 3D framework. Unlike traditional Score Distillation Sampling (SDS) methods, which rely on a single-step noise difference, we supervise latents differences across the entire multi-step editing trajectory. This process enables the distillation of rich semantic information from pretrained 2D diffusion models into 3D representations, yielding photorealistic results. Both theoretical analysis and experiments confirm the effectiveness of our method, which shows strong potential for applications in gaming, film, and interior design. Most importantly, we bridge the gap between 3D generation and 2D editing, paving the way for future research and the integration of advanced 2D editing techniques into 3D generation.

References

- [1] Yuval Alaluf, Omer Tov, Ron Mokady, Rinon Gal, and Amit Bermano. Hyperstyle: Stylegan inversion with hypernetworks for real image editing. In *Proceedings of the IEEE/CVF conference on computer vision and pattern recognition*, pages 18511–18521, 2022. 3, 4
- [2] Mohammadreza Armandpour, Ali Sadeghian, Huangjie Zheng, Amir Sadeghian, and Mingyuan Zhou. Re-imagine the negative prompt algorithm: Transform 2d diffusion into 3d, alleviate janus problem and beyond. *arXiv preprint arXiv:2304.04968*, 2023. 6, 1, 2
- [3] Rui Chen, Yongwei Chen, Ningxin Jiao, and Kui Jia. Fantasia3d: Disentangling geometry and appearance for high-quality text-to-3d content creation. *arXiv preprint arXiv:2303.13873*, 2023. 3, 4
- [4] Wenkai Dong, Song Xue, Xiaoyue Duan, and Shumin Han. Prompt tuning inversion for text-driven image editing using diffusion models. In *Proceedings of the IEEE/CVF International Conference on Computer Vision*, pages 7430–7440, 2023. 4
- [5] Ian Goodfellow, Jean Pouget-Abadie, Mehdi Mirza, Bing Xu, David Warde-Farley, Sherjil Ozair, Aaron Courville, and Yoshua Bengio. Generative adversarial networks. *Communications of the ACM*, 63(11):139–144, 2020. 3
- [6] Yuan-Chen Guo, Ying-Tian Liu, Chen Wang, Zi-Xin Zou, Guan Luo, Chia-Hao Chen, Yan-Pei Cao, and Song-Hai Zhang. threestudio: A unified framework for 3d content generation, 2023. 6
- [7] Amir Hertz, Ron Mokady, Jay Tenenbaum, Kfir Aberman, Yael Pritch, and Daniel Cohen-Or. Prompt-to-prompt image editing with cross attention control. *arXiv preprint arXiv:2208.01626*, 2022. 2, 4, 1
- [8] Martin Heusel, Hubert Ramsauer, Thomas Unterthiner, Bernhard Nessler, and Sepp Hochreiter. Gans trained by a two time-scale update rule converge to a local nash equilibrium. *Advances in neural information processing systems*, 30, 2017. 6
- [9] Jonathan Ho and Tim Salimans. Classifier-free diffusion guidance. *arXiv preprint arXiv:2207.12598*, 2022. 4
- [10] Jonathan Ho, Ajay Jain, and Pieter Abbeel. Denoising diffusion probabilistic models. *Advances in neural information processing systems*, 33:6840–6851, 2020. 3, 4
- [11] Yicong Hong, Kai Zhang, Jiuxiang Gu, Sai Bi, Yang Zhou, Difan Liu, Feng Liu, Kalyan Sunkavalli, Trung Bui, and Hao Tan. Lrm: Large reconstruction model for single image to 3d. *arXiv preprint arXiv:2311.04400*, 2023. 3
- [12] Yukun Huang, Jianan Wang, Yukai Shi, Xianbiao Qi, Zheng-Jun Zha, and Lei Zhang. Dreamtime: An improved optimization strategy for text-to-3d content creation. *arXiv preprint arXiv:2306.12422*, 2023. 1, 3, 4, 8
- [13] Heewoo Jun and Alex Nichol. Shap-e: Generating conditional 3d implicit functions. *arXiv preprint arXiv:2305.02463*, 2023. 3
- [14] Tero Karras, Samuli Laine, Miika Aittala, Janne Hellsten, Jaakko Lehtinen, and Timo Aila. Analyzing and improving the image quality of stylegan. In *Proceedings of the IEEE/CVF conference on computer vision and pattern recognition*, pages 8110–8119, 2020. 3
- [15] Bahjat Kawar, Shiran Zada, Oran Lang, Omer Tov, Huiwen Chang, Tali Dekel, Inbar Mosseri, and Michal Irani. Imagic: Text-based real image editing with diffusion models. In *Proceedings of the IEEE/CVF Conference on Computer Vision and Pattern Recognition*, pages 6007–6017, 2023. 2, 3, 4, 1
- [16] Bernhard Kerbl, Georgios Kopanas, Thomas Leimkühler, and George Drettakis. 3d gaussian splatting for real-time radiance field rendering. *ACM Transactions on Graphics*, 42(4), 2023. 3, 4, 6
- [17] Haoran Li, Haolin Shi, Wenli Zhang, Wenjun Wu, Yong Liao, Lin Wang, Lik-hang Lee, and Pengyuan Zhou. Dreamscene: 3d gaussian-based text-to-3d scene generation via formation pattern sampling. *arXiv preprint arXiv:2404.03575*, 2024. 1, 3, 4, 6
- [18] Haoran Li, Long Ma, Haolin Shi, Yanbin Hao, Yong Liao, Lechao Cheng, and Peng Yuan Zhou. 3d-goi: 3d gan omniversion for multifaceted and multi-object editing. In *European Conference on Computer Vision*, pages 390–406. Springer, 2025. 3
- [19] Yixun Liang, Xin Yang, Jiantao Lin, Haodong Li, Xiaogang Xu, and Yingcong Chen. Luciddreamer: Towards high-fidelity text-to-3d generation via interval score matching. *arXiv preprint arXiv:2311.11284*, 2023. 1, 2, 3, 4, 5, 6, 7
- [20] Chen-Hsuan Lin, Jun Gao, Luming Tang, Towaki Takikawa, Xiaohui Zeng, Xun Huang, Karsten Kreis, Sanja Fidler, Ming-Yu Liu, and Tsung-Yi Lin. Magic3d: High-resolution text-to-3d content creation. In *Proceedings of the IEEE/CVF Conference on Computer Vision and Pattern Recognition*, pages 300–309, 2023. 1, 6, 7
- [21] Gal Metzer, Elad Richardson, Or Patashnik, Raja Giryes, and Daniel Cohen-Or. Latent-nerf for shape-guided generation

- of 3d shapes and textures. In *Proceedings of the IEEE/CVF Conference on Computer Vision and Pattern Recognition*, pages 12663–12673, 2023. 1, 3, 4
- [22] Ben Mildenhall, Pratul P Srinivasan, Matthew Tancik, Jonathan T Barron, Ravi Ramamoorthi, and Ren Ng. Nerf: Representing scenes as neural radiance fields for view synthesis. *Communications of the ACM*, 65(1):99–106, 2021. 4, 6
- [23] Anish Mittal, Anush Krishna Moorthy, and Alan Conrad Bovik. No-reference image quality assessment in the spatial domain. *IEEE Transactions on image processing*, 21(12):4695–4708, 2012. 6
- [24] Daiki Miyake, Akihiro Iohara, Yu Saito, and Toshiyuki Tanaka. Negative-prompt inversion: Fast image inversion for editing with text-guided diffusion models. *arXiv preprint arXiv:2305.16807*, 2023. 3, 4
- [25] Ron Mokady, Amir Hertz, Kfir Aberman, Yael Pritch, and Daniel Cohen-Or. Null-text inversion for editing real images using guided diffusion models. In *Proceedings of the IEEE/CVF Conference on Computer Vision and Pattern Recognition*, pages 6038–6047, 2023. 2, 3, 4
- [26] Alex Nichol, Heewoo Jun, Prafulla Dhariwal, Pamela Mishkin, and Mark Chen. Point-e: A system for generating 3d point clouds from complex prompts. *arXiv preprint arXiv:2212.08751*, 2022. 3, 6
- [27] Ben Poole, Ajay Jain, Jonathan T Barron, and Ben Mildenhall. Dreamfusion: Text-to-3d using 2d diffusion. *arXiv preprint arXiv:2209.14988*, 2022. 1, 3, 4, 5, 6, 7
- [28] Alec Radford, Jong Wook Kim, Chris Hallacy, Aditya Ramesh, Gabriel Goh, Sandhini Agarwal, Girish Sastry, Amanda Askell, Pamela Mishkin, Jack Clark, et al. Learning transferable visual models from natural language supervision. In *International conference on machine learning*, pages 8748–8763. PMLR, 2021. 6
- [29] Robin Rombach, Andreas Blattmann, Dominik Lorenz, Patrick Esser, and Björn Ommer. High-resolution image synthesis with latent diffusion models. In *Proceedings of the IEEE/CVF conference on computer vision and pattern recognition*, pages 10684–10695, 2022. 1, 3, 4, 6, 7
- [30] Chitwan Saharia, William Chan, Saurabh Saxena, Lala Li, Jay Whang, Emily L Denton, Kamyar Ghasemipour, Raphael Gontijo Lopes, Burcu Karagol Ayan, Tim Salimans, et al. Photorealistic text-to-image diffusion models with deep language understanding. *Advances in Neural Information Processing Systems*, 35:36479–36494, 2022. 1
- [31] Tianchang Shen, Jun Gao, Kangxue Yin, Ming-Yu Liu, and Sanja Fidler. Deep marching tetrahedra: a hybrid representation for high-resolution 3d shape synthesis. *Advances in Neural Information Processing Systems*, 34:6087–6101, 2021. 4, 6
- [32] Yichun Shi, Peng Wang, Jianglong Ye, Mai Long, Kejie Li, and Xiao Yang. Mvdream: Multi-view diffusion for 3d generation. *arXiv preprint arXiv:2308.16512*, 2023. 3
- [33] Jiaming Song, Chenlin Meng, and Stefano Ermon. Denoising diffusion implicit models. *arXiv preprint arXiv:2010.02502*, 2020. 1, 3, 4
- [34] Jiayang Tang, Jiawei Ren, Hang Zhou, Ziwei Liu, and Gang Zeng. Dreamgaussian: Generative gaussian splatting for efficient 3d content creation. *arXiv preprint arXiv:2309.16653*, 2023. 1, 3, 4
- [35] Omer Tov, Yuval Alaluf, Yotam Nitzan, Or Patashnik, and Daniel Cohen-Or. Designing an encoder for stylegan image manipulation. *ACM Transactions on Graphics (TOG)*, 40(4):1–14, 2021. 3, 4
- [36] Tengfei Wang, Yong Zhang, Yanbo Fan, Jue Wang, and Qifeng Chen. High-fidelity gan inversion for image attribute editing. In *Proceedings of the IEEE/CVF Conference on Computer Vision and Pattern Recognition*, pages 11379–11388, 2022. 3, 4
- [37] Zhengyi Wang, Cheng Lu, Yikai Wang, Fan Bao, Chongxuan Li, Hang Su, and Jun Zhu. Prolificdreamer: High-fidelity and diverse text-to-3d generation with variational score distillation. *Advances in Neural Information Processing Systems*, 36, 2024. 1, 3, 6, 7
- [38] Tianyi Wei, Dongdong Chen, Wenbo Zhou, Jing Liao, Weiming Zhang, Lu Yuan, Gang Hua, and Nenghai Yu. E2style: Improve the efficiency and effectiveness of stylegan inversion. *IEEE Transactions on Image Processing*, 31:3267–3280, 2022. 3
- [39] Zike Wu, Pan Zhou, Xuanyu Yi, Xiaoding Yuan, and Hanwang Zhang. Consistent3d: Towards consistent high-fidelity text-to-3d generation with deterministic sampling prior. In *Proceedings of the IEEE/CVF Conference on Computer Vision and Pattern Recognition*, pages 9892–9902, 2024. 3
- [40] Xianghui Yang, Huiwen Shi, Bowen Zhang, Fan Yang, Jiacheng Wang, Hongxu Zhao, Xinhai Liu, Xinzhou Wang, Qingxiang Lin, Jiaao Yu, et al. Tencent hunyuan3d-1.0: A unified framework for text-to-3d and image-to-3d generation. *arXiv e-prints*, pages arXiv–2411, 2024. 3
- [41] Taoran Yi, Jiemin Fang, Guanjun Wu, Lingxi Xie, Xiaopeng Zhang, Wenyu Liu, Qi Tian, and Xinggang Wang. Gaussian-dreamer: Fast generation from text to 3d gaussian splatting with point cloud priors. *arXiv preprint arXiv:2310.08529*, 2023. 6, 7
- [42] Xin Yu, Yuan-Chen Guo, Yangguang Li, Ding Liang, Song-Hai Zhang, and Xiaojuan Qi. Text-to-3d with classifier score distillation. *arXiv preprint arXiv:2310.19415*, 2023. 3

Enhanced 3D Generation by 2D Editing

Supplementary Material

6. Supplementary Methods

6.1. More connections between 2D editing and SDS text-to-3D methods

6.1.1 Imagic vs. ProlificDreamer

Imagic [15] is a prominent method in text-based 2D editing, with its editing process divided into three main stages. Initially, it aligns the target text embedding y_{tgt} with a pre-trained diffusion model [29, 30] using a reconstruction loss to ensure alignment with the input image. In the second stage, both the image and the optimized text embedding y_{opt} are fixed, and the diffusion model undergoes fine-tuning through the reconstruction loss to enhance alignment. These two stages align the input image, text embedding and the diffusion model, facilitating the image inversion as discussed in Section 2.2. The final stage focuses on editing: the interpolated target text embedding y_{tgt} and optimized text embedding y_{opt} are then fed into the fine-tuned diffusion model to produce the edited image. By aligning all three components in a high-dimensional space, Imagic ensures that the edited image captures both the content of the original image and the intent of the editing text, resulting in high-quality editing outcomes.

ProlificDreamer [37] utilizes a two-stage optimization in each iteration. In the first stage, it fixes the input image and fine-tuned pretrained diffusion model by minimizing $\mathbb{E}_{t, \epsilon, c} [|\epsilon_\phi(x_t, t, c, y) - \epsilon|_2^2]$. In the second stage, the parameters ϕ of the diffusion model are frozen, and the 3D representation (input image) is optimized using the traditional SDS loss [27].

Comparing these two methods reveals that ProlificDreamer essentially conducts an image editing process in each iteration. Like in Imagic, the first stage involves aligning the input image with the text embedding and the diffusion model. In the second stage, the input image is edited using the fine-tuned diffusion model and the target text embedding, optimizing towards the desired distribution for the text-guided rendered image. At this point, the noise vector from the pretrained model $\epsilon_{pretrain}(x_t, t, y)$ balances the content of the input image with the editing text, ensuring a stable and high-quality optimization direction. Consequently, the resulting 3D model achieves excellent outcomes.

6.1.2 Appropriate farthest timestep

In **Prompt2Prompt** [7], it has been observed that introducing too much target text information during the editing process, without maintaining consistency with the original im-

age, can cause the edited image to significantly deviate from the input. Conversely, prioritizing consistency too heavily may suppress the intended effects of the editing text, leading to inaccurate edits. This observation corresponds with our ablation experiments concerning the farthest timestep and step size. If the farthest timestep is too large or the number of steps is too high, consistency diminishes, destabilizing the optimization process and leading to the Janus (multi-head) problem, where the same text information is expressed in multiple directions. On the other hand, excessively preserving consistency, such as using a very small farthest timestep and fewer steps, can yield results that do not align with the intended textual modifications. Therefore, we advocate for a **moderate** farthest timestep. This view is supported by findings from **DreamTime** [12], which emphasize the importance of information provided at intermediate diffusion timesteps for effective 3D optimization.

6.2. Easily combine with other methods.

Perp-Neg [2] addresses the Janus (multi-head) problem in SDS [27] by using distinct text descriptions for different camera viewpoints (e.g., front, side, back views) as guidance. It employs negative text techniques to suppress undesired expressions from alternate viewpoints. The primary formula used in Perp-Neg is as follows:

$$\begin{cases} \epsilon_\phi^{pos_v} = \epsilon_\phi(x_t, t, y_{pos}^{(v)}) - \epsilon_\phi(x_t, t, \emptyset) \\ \epsilon_\phi^{neg_v^{(i)}} = \epsilon_\phi(x_t, t, y_{neg}^{(v)}(i)) - \epsilon_\phi(x_t, t, \emptyset) \\ \tilde{\epsilon}_\phi^{PN}(x_t, t, v, y) = \epsilon_\phi(x_t, t, \emptyset) + \omega[\epsilon_\phi^{pos_v} - \sum_i \omega_v^{(i)} \epsilon_\phi^{neg_v^{(i)\perp}}] \end{cases} \quad (15)$$

where $y^{(v)}$ is the positive or negative text embedding at viewpoint v . $\epsilon_\phi^{neg_v^{(i)\perp}}$ refers the perpendicular component of $\epsilon_\phi^{neg_v^{(i)}}$ on the $\epsilon_\phi^{pos_v}$. And $\omega_v^{(i)}$ represent the i -th weights of negative prompts.

We can seamlessly integrate this method into our pipeline by substituting $\tilde{\epsilon}_\phi(x_t, t, y, \emptyset)$ to $\tilde{\epsilon}_\phi^{PN}(x_t, t, v, y)$.

Reconstructive generation is a technique used in Formation Pattern Sampling (FPS) [17] to expedite the creation of surface textures. This method primarily employs a single-step denoising approach to generate images during the final stages of 3D representation optimization, where there is already good consistency. The process then effectively transforms the generation task into a reconstruction task. To enhance this, we replace the **single-step** denoising with **multi-step** denoising along the denoising trajectory, enabling the generation of edited images with detailed textures. We can

similarly utilize reconstruction methods to further accelerate the generation process.

7. Supplementary Experiments

In this section, additional qualitative experimental results are provided in Section 7.1. A more detailed qualitative comparison with ISM [19] is available in Section 7.2. The generation process of GE3D is showcased in Section 7.3, and an ablation study comparing the use of only $x_0 - \tilde{x}_0$ with GE3D is presented in Section 7.4.

7.1. More results

As demonstrated in Figures 11 and 12, we provide additional examples of 3D generation from complex prompts in real-world scenarios. GE3D not only showcases its ability to produce photorealistic 3D content but also exhibits excellent generalization performance.

7.2. Detailed Comparison with ISM

As shown in Figure 13, we present a frame-by-frame comparison with ISM [19] from multiple viewpoints. As quantitatively analyzed in Section 3.2, ISM utilizes a single-step editing process at a relatively large timestep to preserve coarse-grained information. Consequently, while its generated content aligns well with the text, it lacks fine-grained details. This deficiency is particularly noticeable in the textures of human faces and animal fur, where ISM struggles to produce ultra-high-quality 3D content. By employing multi-step editing, our approach GE3D extracts information of varying granularities from the diffusion model, resulting in superior quality in the generated content.

7.3. Generation Process of GE3D

As illustrated in Figure 14, we demonstrate the generation process of GE3D by displaying the results of pseudo-GT [19] for images under different denoising diffusion trajectory steps i and iterations k (with a total of 3000 iterations, 6 diffusion steps, and a step size between 60 and 80). From left to right, the diffusion model initially emphasizes shape information at larger timesteps, resulting in simpler and smoother textures like fur. However, as shown on the far right, the model gradually provides more fine-grained details, such as realistic colors and textures. This progression supports our analysis in the main text that general content generation occurs within 500 to 1000 steps, with subsequent steps focused on refining surface textures to achieve higher-quality 3D results.

7.4. Using only x_0

As shown in Figure 10, we evaluated the outcomes of optimizing the 3D representation using only $x_0 - \tilde{x}_0$. Despite requiring the same computational effort as our full multi-step editing process, this approach is more susceptible to

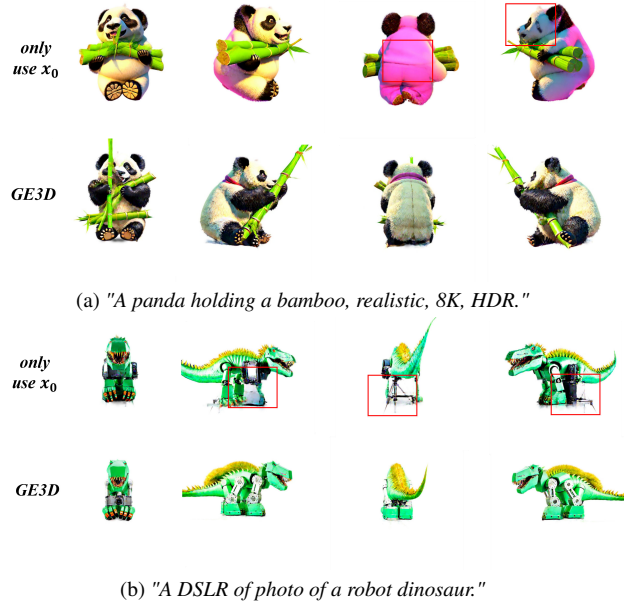


Figure 10. Comparison with methods using only $x_0 - \tilde{x}_0$. This method utilizes excessive fine-grained details, which can lead to the production of unreasonable content.

the Janus problem—even with the incorporation of the Perp-Neg [2] module—and tends to produce unreasonable content. This issue arises because \tilde{x}_0 retains excessive fine-grained details. At the initial generation stage, this can lead to the generation of the same textual content in multiple directions, resulting in irrational outcomes.

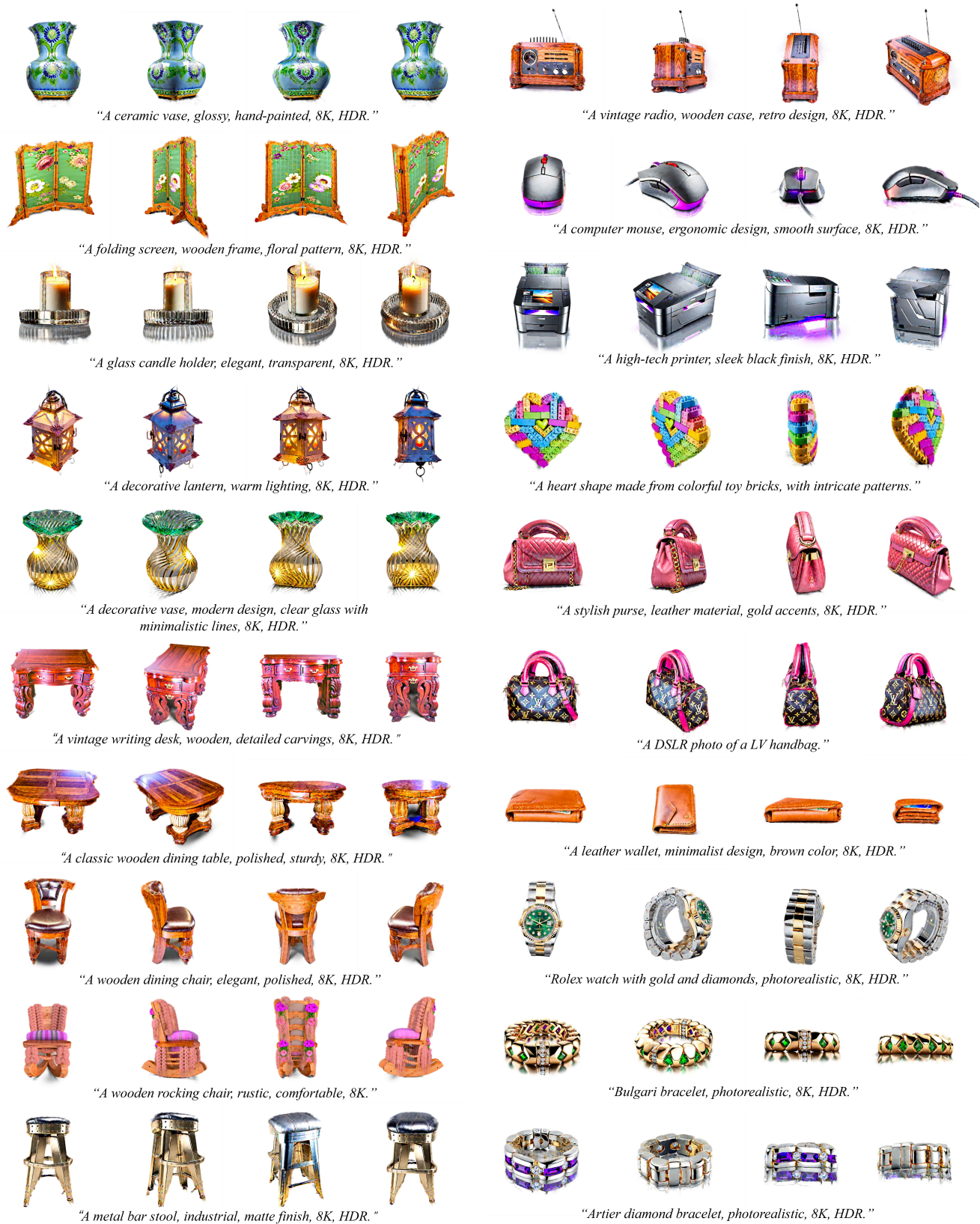


Figure 11. More quantitative results of GE3D.



"A soft plush toy of a cute puppy with floppy ears and a wagging tail."



"Head of Thanos with a gold helmet, photorealistic, 8K, HDR."



"A panda cub wearing a flower crown."



"Black Panther in Marvel, head, photorealistic, 8K, HDR."



"A highly detailed octopus, underwater, realistic, 8K, HDR."



"Thor; head, photorealistic, 8K, HDR."



"A western dragon with fire, covered in scales, 8K."



"Spider Man, green head, photorealistic, 8K, HDR."



"A cheetah in racing goggles, realistic, 8K, HDR."



"Uchiha Sasuke, head, photorealistic, 8K, HDR."



"A panda wearing sunglasses, realistic, 8K, HDR."



"Marilyn Monroe's head with curly hair, photorealistic, 8K, HDR."



"A high-detail corgi, realistic, 8K, HDR."



"Michael Jackson, photorealistic, 8K, HDR."



"A giraffe with a scarf, cozy, realistic, 8K, HDR."



"Buzz Lightyear in Disney, photorealistic, 8K, HDR."



"Mickey Mouse in Disney, photorealistic, 8K, HDR."



"Aladdin with a magic lamp, photorealistic, 8K, HDR."

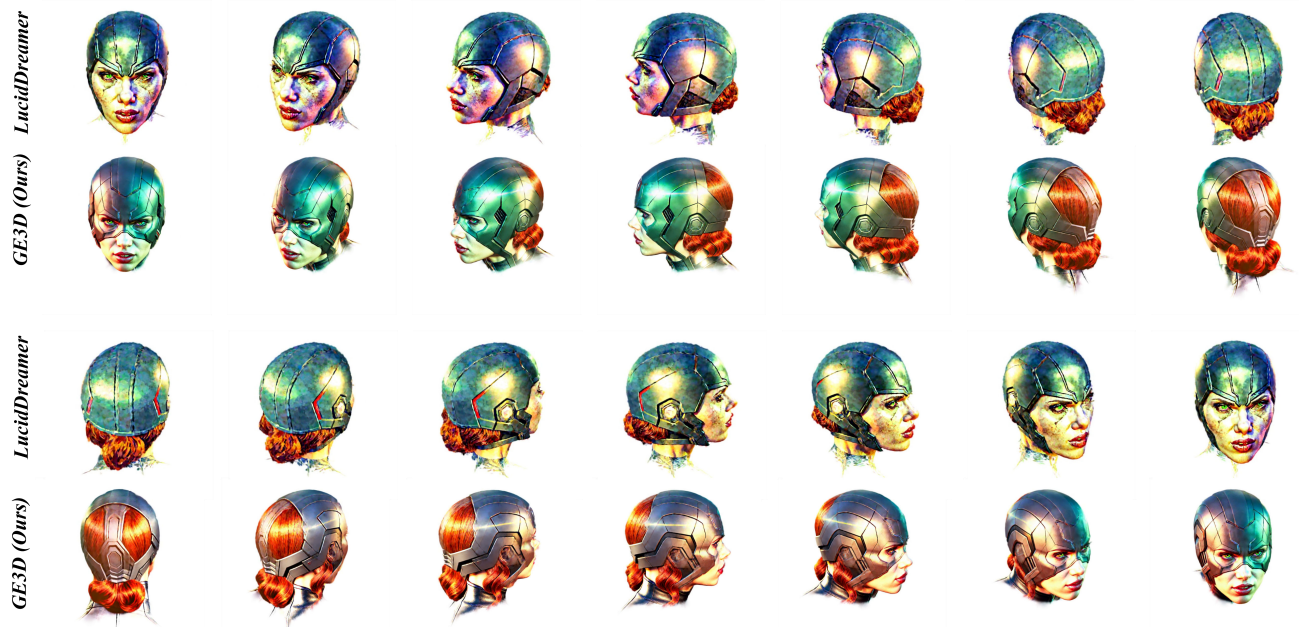


"Pinocchio in Disney, photorealistic, 8K, HDR"



"Harry Potter with a wand, photorealistic, 8K, HDR."

Figure 12. More quantitative results of GE3D.



(a) "Black Panther in Marvel, head, photorealistic, 8K, HDR."



(b) "A delicious hamburger."

Figure 13. Detailed comparison between GE3D and ISM [19]. The 3D content generated by GE3D is of higher quality and contains more detailed features.



Figure 14. The generation process of GE3D.